MRS Communications (2023) 13:1238–1243

https://doi.org/10.1557/s43579-023-00438-y

MRS Communications

Research Letter

Novel MgC_2O_4 cathode material for its application in Mg^{2+}/Li^+ hybrid ion batteries: Synthesis and electrochemical performance

Jesús Guzmán-Torres, Edgar González-Juárez, Lorena L. Garza-Tovar, Eduardo M. Sánchez-Cervantes, Facultad de Ciencias Químicas, Universidad Autónoma de Nuevo León, Av. Universidad S/N Ciudad Universitaria, C.P. 66451 San Nicolas de los Garza, Nuevo León, Mexico

Address all correspondence to Eduardo M. Sánchez-Cervantes at **eduardo.sanchezcv@uanl.edu.mx**

(Received 18 March 2023; accepted 9 August 2023; published online: 30 August 2023)

Abstract

The magnesium oxalate (MgC_2O_4) cathode material was synthesized via a dissolution route. This material exhibited higher electrochemical performance in Mg^{2+}/Li^+ hybrid ion batteries (MLIBs) compared with magnesium ion rechargeable batteries (MIBs) that were prepared. In MLIBs, this material showed a discharge capacity of 292, 226, 186, 134, 99, 71, and 32 mAh g^{-1} after 65 cycles at 2, 10, 20, 50, 100, 200, and 400 mA g^{-1}, respectively. Then, the MgC_2O_4 material has the potential to be applied as a cathode in energy storage and conversion devices, such as MLIBs.

Introduction

Today, human, and industrial activities generate significant CO_2 emissions to a level that has raised the temperature of the planet by 1°C. Without new government regulations, responsiveness among citizens, and clean and renewable technologies, global warming of 1.5°C is projected by 2040. In this context, the demand for energy storage and conversion devices has grown exponentially in recent years. Nonetheless, solar, wind, and hydro energy sources have become insufficient to satisfy the increasing demand due to intermittent energy storage.[1] Lithium-ion rechargeable batteries (LIBs) are popular due to their outstanding electrochemical properties. Additionally, they have been widely used in the industrial sector with endless applications ranging from electronic devices such as cell phones, tablets, and computers to electric chairs, cars, and boats since the last century.[2] However, it is known that LIBs have safety problems when using lithium anodes, which can lead to dendritic growth and flammable electrolytes, posing safety risks over the years.[3] In this sense, magnesium-ion rechargeable batteries (MIBs) have gained great interest as a potential substitute for LIBs, as they have similar energy densities and greater global abundance of resources. Magnesium (Mg) is the 8th most abundant element and the 3rd most plentiful element dissolved in seawater, and it does not have safety issues.[4] Another important advantage is that Mg can achieve a high theoretical specific capacity of 2205 mAh g^{-1} and volumetric capacities as high as 3833 mAh cm^{-3}, which are comparable to Li metal batteries. It is also well known that due to their abundance in the earth's crust (2.9%), they are a low-cost alternative. Nevertheless, they do have some disadvantages, such as slow diffusion kinetics due to strong Coulombic interactions with the host material and difficulties in the insertion/extraction of divalent Mg^{2+}, resulting in rapid capacity decay of cathode materials, as well as problems associated with the passivation of Mg with electrolytes, which currently postpone its commercial application. On the other hand, Mg^{2+}/Li^+ hybrid ion batteries (MLIBs) aim to improve the electrochemical performance of both separately by combining the properties of both their electrodes and electrolytes. This approach can result in storage mechanisms such as Daniel, rocking-chair, and co-intercalation types.[5] MLIBs are generally composed of Li^+ and Mg^{2+} intercalation cathodes, along with double insertion materials that combine the high capacity of cathodes with dendrite-free anodes based on metallic Mg. While cathodes prepared with metal oxides have adapted well to MLIBs, the reported synthesis methods are considered uneconomical due to their high-temperature requirements or expensive starting materials. In this sense, transition metal oxalates are considered sustainable energy storage materials because oxalate ions can be produced from CO_2 through synthetic and biosynthetic processes. Therefore, metal oxalates could contribute to reducing the overall atmospheric CO_2 levels if the energy used to convert CO_2 into $C_2O_4^{2-}$ comes from a low-carbon emitting energy source.[6] The most common transition metal oxalate complexes are based on first-row divalent transition metals in the dihydrated form $M^{2+}(C_2O_4)\cdot 2H_2O$ with different polymorphisms, and many have been studied individually or mixed, for example oxalates based on Mn, Fe, Co, Zn.[7]

To our knowledge, no previous reports have used magnesium oxalate as a novel cathode material in MLIBs. In this study, we propose a preliminary investigation of MgC_2O_4 synthesized from low-cost materials via a dissolution route. The resulting product was tested as a cathode in MLIBs and exhibited excellent electrochemical properties, including a high experimental specific capacity (≈ 284 mAh g^{-1}), compared to the theoretical specific capacity (≈ 239 mAh g^{-1}), and a coulombic efficiency above 99%.

Experimental section

Synthesis of MgC_2O_4

MgC_2O_4 was synthesized using oxalic acid, $C_2H_2O_4$, (anhydrous ≥ 99%; Sigma-Aldrich) and magnesium acetate tetrahydrate, $Mg(CH_3COO)_2{\cdot}4H_2O$, (ACS reagent ≥ 99%; Sigma-Aldrich) as raw materials (see Table S1 in supplementary information). The ratio of 1:1 mol% was weighed and mixed by the following reactions:

$$H_2C_2O_4 + Mg(CH_2COO)_2 \cdot 4H_2O \rightarrow MgC_2O_4 \cdot 2H_2O + 2CH_3COOH \cdot 2H_2O \quad (1)$$

$$MgC_2O_4 \cdot 2H_2O + 2CH_3COOH \cdot 2H_2O \xrightarrow{\Delta 140\,^\circ C} MgC_2O_4 \cdot 2H_2O \quad (2)$$

$$MgC_2O_4 \cdot 2H_2O \xrightarrow{\Delta 250\,^\circ C} MgC_2O_4 \quad (3)$$

The reaction was carried out by dissolution method, where in the first step (Eq. 1), the mixture was prepared by dissolving 3 g of oxalic acid anhydrous and magnesium acetate tetrahydrate in 30 ml of distilled water, and 5 ml of absolute ethanol were added to reduce particle size, with continuous stirring for 2 h. Afterwards, the solution was heated at 140 °C to eliminate the by-product formed (acetic acid/Eq. 2) until the total evaporation of the liquid part. The resulting white powder was subsequently heated into a vacuum oven at 250 °C for another 24 h for total removal of water (Eq. 3).

Structural, morphological, and thermal characterization

The Neoscope JCM-6000 instrument from JEOL was used to analyze the particle size and morphology. The x-ray diffraction analysis (XRD) for the determination of the crystalline structure and phase identification of MgC_2O_4 was performed using a D2-Phaser instrument from Bruker equipped with a CuKα radiation source (λ = 1.5418 Å). Fourier-transform infrared spectroscopy (FTIR) was conducted on an Interspec 200-X instrument within the wave number range of 400–4000 cm^{-1}, with KBr pellets used as a reference for sample measurements. To obtain the DTA curves of MgC_2O_4 and raw materials, a Shimadzu differential thermal analyzer (model DTA-50) was utilized under a nitrogen atmosphere (10 ml min^{-1}) at a heating rate of 10 °C min^{-1}. The temperature range was 30–800 °C for MgC_2O_4 and 30–300 °C for the raw materials, with a sample mass of 3.0 ± 0.05 mg and platinum micro pans used for all measurements.

Preparation of electrolyte

The all-phenyl complex (APC) electrolyte was prepared by reacting stoichiometric amounts of $AlCl_3$ (anhydrous powder, 99.99%, Sigma-Aldrich) and phenylmagnesium chloride (2.0 M in THF, Sigma-Aldrich) in THF (anhydrous, ≥ 99.9%, Sigma-Aldrich). A 1.25 M concentration of LiCl (powder, ≥ 99.98%, Sigma-Aldrich) was added to this solution as a source of lithium. The anode was made of a Mg disc, while a glass microfiber filter was employed as the separator. The final concentration of the hybrid electrolyte was 0.4 M APC/1.25 M LiCl.

Electrochemical measurements

Half cells were prepared using synthesized cathodic active material MgC_2O_4. The cathodes were prepared via the mixture of 70 wt% active material, 20 wt% carbon black (Carbon Super P, TIMCAL) and 10 wt% Polytetrafluoroethylene (powder 35 µm particle size, Sigma-Aldrich), and the solid mixture was compressed on a stainless-steel mesh. The electrochemical test was achieved using a VMP3 multipotentiostat (Biologic Science Instrument). Coin cells CR2032 type SS316 were selected for their good electrochemical properties.[8] These cells were assembled in a dry box (Omni-Lab 0210, VAC) filled with Argon and H_2O < 1 ppm.

Results and discussion

X-ray diffraction studies

Figure 1(a) shows the results obtained by XRD of MgC_2O_4 (see Figure S1(a) in supplementary information that includes the XRD pattern of raw materials). The diffraction peaks coincide with the PDF database ICDD 00-026-1222 corresponding to a type of monoclinic structure with a space group of C2/c. The compound name is magnesium oxalate, with side lengths a, b, and c = 9.413 Å, 6.229 Å, 5.724 Å, respectively, and angles $\alpha = \gamma = 90°$, $\beta = 96.47°$. The cell volume of the unit cell is 333.49 $Å^3$ and $Z = 4$ formulas per unit cell. The morphology of MgC_2O_4, observed in the inset in Fig. 1(a), was obtained through SEM. It can be clearly seen that the synthesized material has a cylindrical rod morphology with a micrometer-scale size.[9]

Scherrer's equation (Eq. 4) was used to determine the average size of the crystallites, considering the three highest intensity peaks. The equation involves several variables: D represents the crystal grain size, m is the full width at half-maximum (FWHM), λ is the wavelength of the X-rays, θ is the diffraction angle, and K is the Scherrer constant, expressed in radians with a value of 0.89. The equation is as follows:

$$D = \frac{K\lambda}{m\cos\theta} \quad (4)$$

To ensure unit consistency throughout the calculation process, it is recommended that the FWHM value be expressed in radians.[10] Table S2 in supplementary information provides the crystallite sizes of the three maximum intensities. The average size of the crystallites was found to be 26.88 nm based on the FWHM value obtained from the XRD pattern. The maximum size was 32.69 nm, and the minimum size was 19.54 nm.

Figure 1(b) displays the FTIR spectrum of the synthesized MgC_2O_4. The powder technique[11] utilized in this analysis allowed for the identification of absorption bands. The main infrared peaks of MgC_2O_4 and their characteristic functional group bands, as well as the FTIR spectrum of the raw materials, can be found in supplementary information, in Table S3 and Fig. S1(b), individually. The absorption band observed at 3416 cm^{-1} in the FTIR spectrum corresponds to the O–H

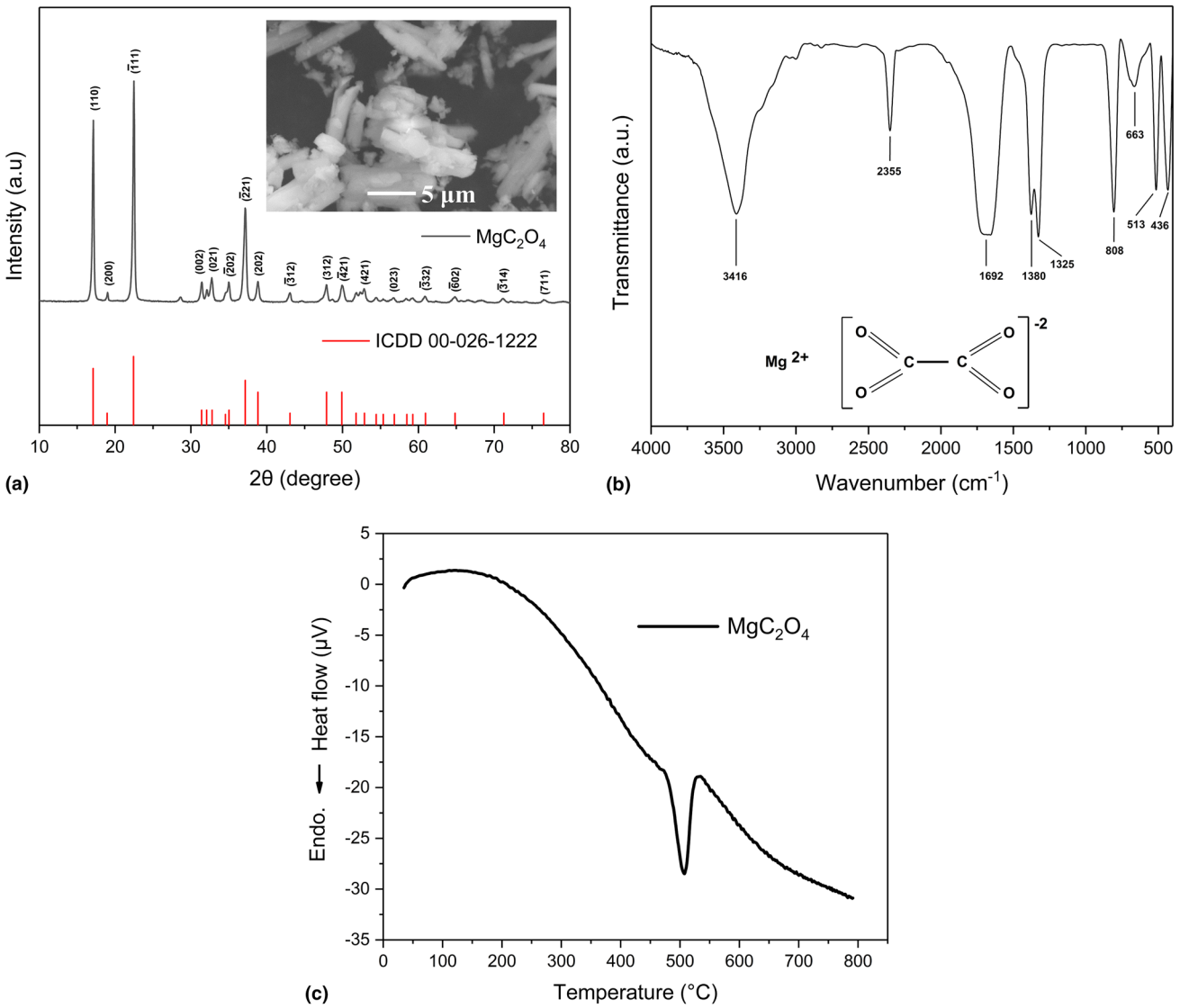

Figure 1. (a) XRD pattern of MgC_2O_4; Inset: SEM image of the solid, (b) FTIR spectrum of MgC_2O_4; Inset: Structure of the molecule, and **c** DTA curve of MgC_2O_4.

bond, which is attributed to the presence of water absorbed by the sample.[12] In contrast, the band observed at 2355 cm^{-1} can be associated with the stretch vibrations of the atoms in the C–O bond; it is attributed to gaseous CO_2 absorbed in the analyzed powder.[13] The presence of the asymmetric stretch of C–O in the MgC_2O_4 complex was confirmed by the absorption band at 1692 cm^{-1}. Meanwhile, the functional groups at 1380 and 1325 cm^{-1} were attributed to the symmetric stretch of C–O and the scissoring stretch of O–C–O, respectively.[14] Another absorption band observed at 808 cm^{-1} was attributed to the strain stretch of C–O–C.[15] The fingerprint bands of the MgC_2O_4 salt appeared at 663, 513, and 436 cm^{-1}, which were associated with the stretch bending of water vibration and Mg–O stretch.[16]

The DTA curve of MgC_2O_4 is shown in Fig. 1(c) (see Fig. S1(c) in supplementary information for raw materials results). As can be observed from the thermogram in Fig. 1(c), only one endothermic event is exhibited at 500 °C, corresponding to MgC_2O_4 first decomposition to produce $MgCO_3$ and CO. The absences of low temperature thermal events indicates that there is no presence of crystallization (hydrates) or absorbed water (moisture). This indicates that there is no presence of water hydrates.[17,18]

Electrochemical performance

Cyclic voltammetry (CV) curves are present in Fig. 2(a). The reaction mechanism can be described by Eq. 5:

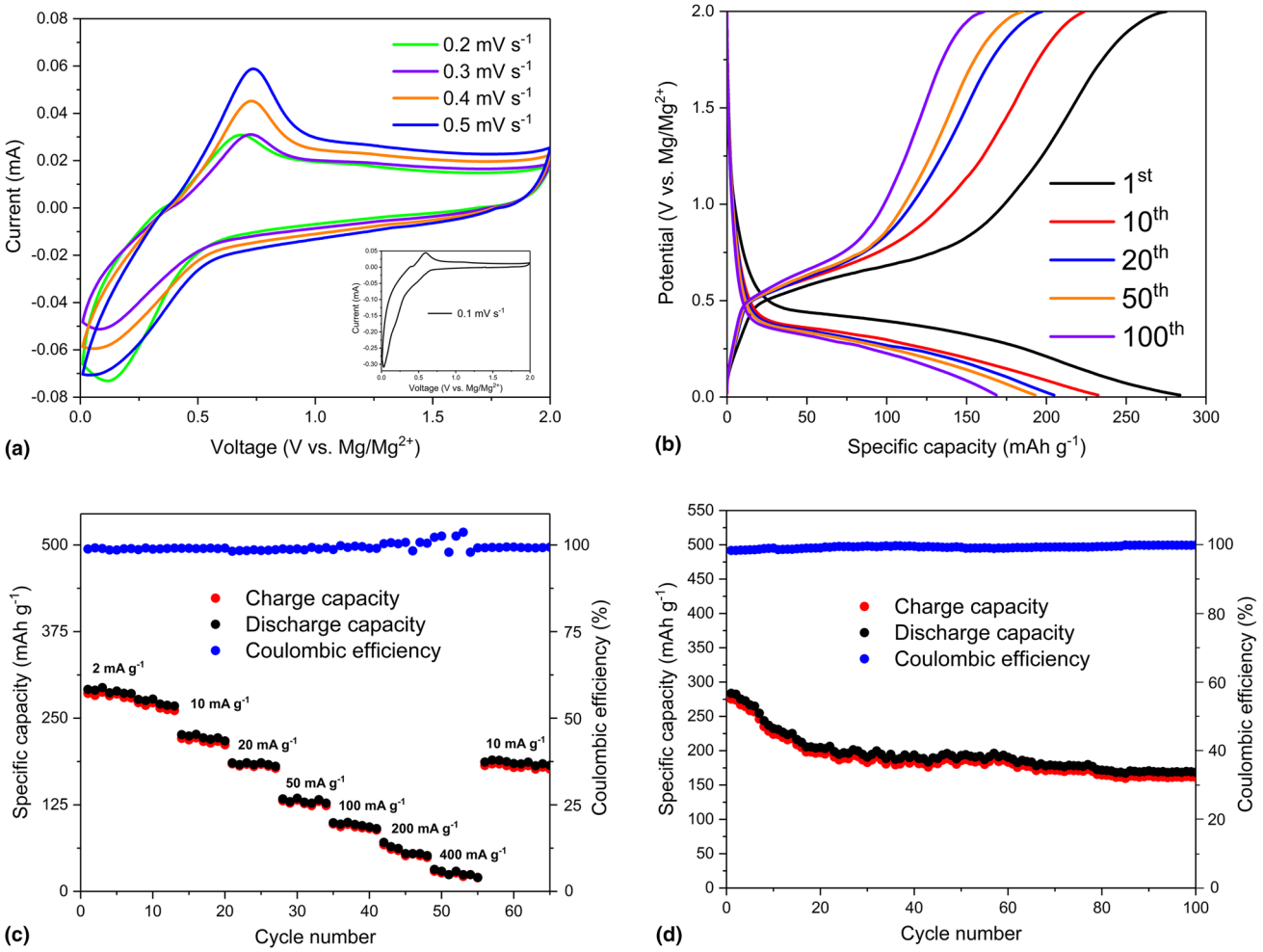

Figure 2. Electrochemical performances of the Mg || 0.4 M APC/1.25 M LiCl || MgC_2O_4 batteries cycling in the voltage range of 0.01–2.0 V. (a) CV curves at different scan rates; Inset: First cycle at 0.1 mV s^{-1}, (b) Galvanostatic charge/discharge profiles at 10 mA g^{-1}, and (c) Rate performance at current densities from 2 to 400 mA g^{-1}; and (d) Cycling performance at 10 mA g^{-1}.

$$MgC_2O_4 + 2Li^+ + 2e^- \overset{\text{charge/dicharge}}{\longleftrightarrow} Mg + Li_2C_2O_4 \quad (5)$$

The CV curves reveal two peaks in charge and discharge at 0.6–0.8 and 0.01–0.25 V, respectively, due to surface layer formation in the first cycle [Inset Fig. 2(a)] and conversion reaction in subsequent cycles at different scan rates attributed to the Mg^{2+}/Mg^0 accompanying with the decomposition of $Li_2C_2O_4$, similar to analogues reported in the literature.[19–21] To further illustrate the electrochemical properties, the charging and discharging profiles were performed at a current density in the Mg || 0.4 M APC/1.25 M LiCl || MgC_2O_4 batteries, using a dual salt electrolyte.[22] The cell subjected to a continuous current density of 10 mA g^{-1}, achieved a high discharge capacity of 284 mAh g^{-1} at first cycle to later achieve specific capacities of 232, 205, 193 and 167 mAh g^{-1} at the 10, 20, 50 and 100 cycles [Fig. 2(b)], remaining above the results obtained in the Mg || 0.4 M APC || MgC_2O_4 batteries (see Fig. S2(a–d) in supplementary information).

The battery displayed discharge capacities at different current densities ranging from 2 to 400 mA g^{-1}, as seen in Fig. 2(c). The discharge capacities recorded through the first, twenty-first, thirty-fifth, forty-second, and forty-ninth cycles were 292, 186, 99, 71, and 32 mAh g^{-1}, correspondly. Hence, when cycle 65 ended, the battery regained up to 83% of its initial capacity. These results suggest a progressive decrease in battery performance as the cycle number increases, since undergoing high-rate discharge cycles, the MgC_2O_4 cathode showed remarkable stability and reversibility. This shows that the battery can maintain its functionality over an extended period, making it a reliable energy storage device. However, when subjected to greater cycling, it was observed that only after 85 cycles did it remain sufficiently stable, reaching a discharge capacity of 167 mAh g^{-1} at the end of cycle 100 with a capacity retention of 57% [Fig. 2(d)]. The findings of this study demonstrate that oxalate-based cathode materials exhibit good electrochemical performance and low cost per gram comparable to anodes based on Zinc,[23] Tin,[24] Nickel,[25] Copper,[26]

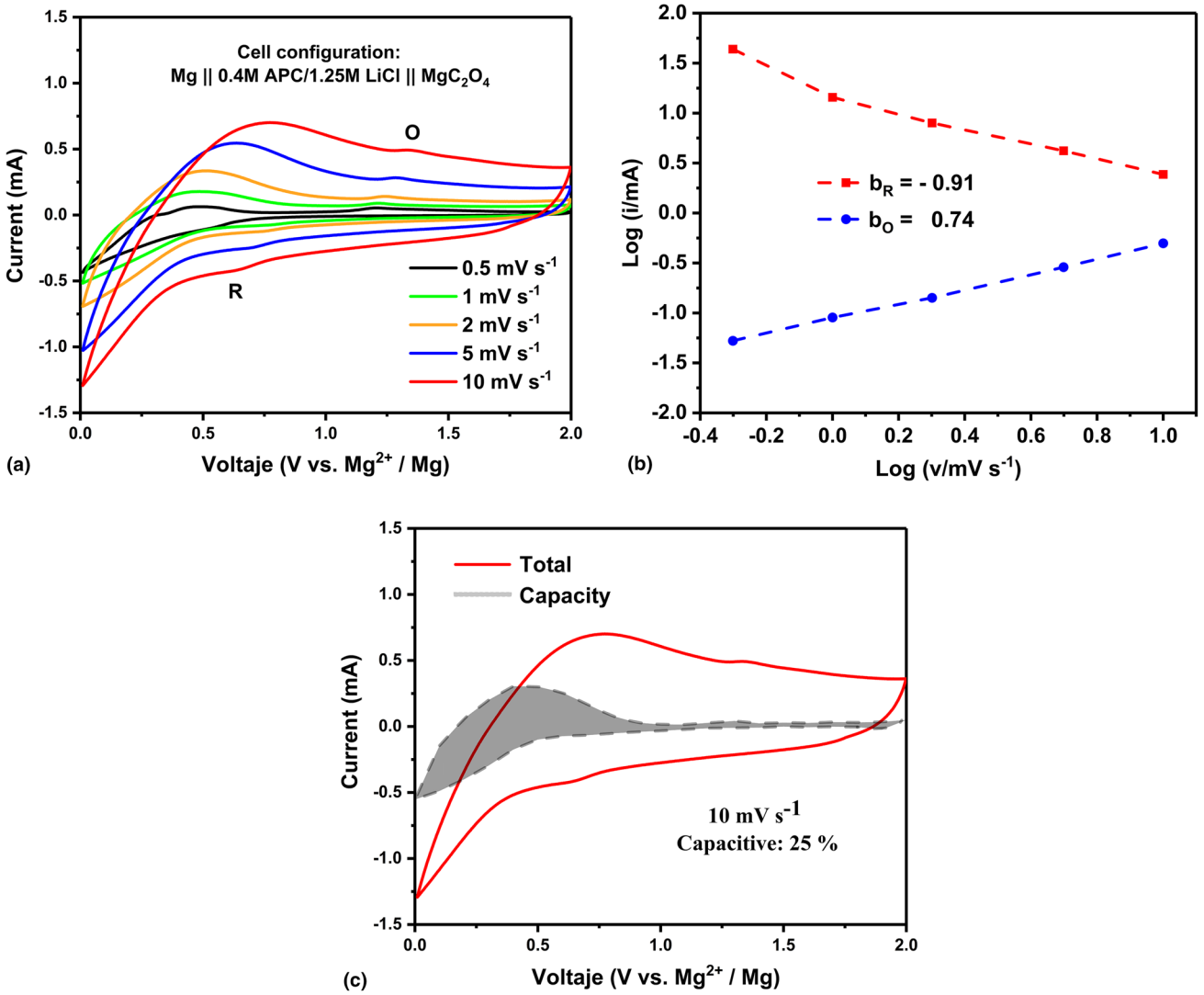

Figure 3. (a) CV curves of the MgC_2O_4 MLIB cell at different scan rates, (b) linear fitting of the Log (*i*) vs. Log(*v*) plots, scan rates were varied from 0.5 to 10 mV s^{-1}, and (c) separation of the capacitive (shadow area) and diffusion-controlled charge contributions data at the scan rate of 10 mV s^{-1} in the MgC_2O_4 MLIB cell configuration.

Manganese,[27] Cobalt,[28] and Iron,[29] as shown in Table S4 in the supplementary information.

In Fig. 3(a), the CV curves for MgC_2O_4 cell are displayed at various scan rates. As scan rate increases, the redox peaks shift due to the diffusion-controlled nature of the redox process. At a scan rate of 10 mV s^{-1}, the material exhibited a reduction peak around 0.6 V vs. Mg^{2+}/Mg and an oxidation peak of approximately 1.3 V. It is well known that the maximum current obeys the power law relationship with the scan speed and can be determined by Dunn's method (Eq. 6).[30]

$$i = ab^{\upsilon} \tag{6}$$

A b value of 0.5 indicates diffusion-controlled behavior, while a b value of 1.0 indicates a capacitive process. The slope of Log(*i*) versus Log(*m*) gives the b value, as shown in Fig. 3(b). The b value analysis was performed using CV data between 0.3 and 1.7 V. The b values of the reduction (0.91) and oxidation (0.74) peaks for MgC_2O_4 cell. The total current containing contributions from the two types of processes can be described via following Eqs. 7 and 8:

$$i(V) = k_1\upsilon^{1/2} + k_2\upsilon \tag{7}$$

or

$$\frac{i(V)}{\upsilon^{1/2}} = k_1 + k_2\upsilon^{1/2} \tag{8}$$

By drawing the plots of $i/\upsilon^{1/2}$ vs $\upsilon^{1/2}$ at the discharge and charge state (see Fig. S3 in supplementary information), the value of k_1 and k_2 at a fixed voltage can be calculated through the intercept and the slope of the curves, respectively. Consequently, by determining k_1 and k_2, the fraction of the current

due to each of these contributions can be quantified at specific potentials. According to the calculated result, Fig. 2(c) shows that about 25% of the total capacity is pseudocapacitance obtained at a scan rate of 10 mV s^{-1}.

Finally, it is important to comment that under the line of research on the development of new materials for energy storage, materials for cathodes based on oxalate have potential applications in multivalent ion batteries. However, more research is needed to investigate and optimize the performance of these materials.

Conclusions

In this work, we used oxalic acid and magnesium acetate tetrahydrate as a low-cost raw material by applying the dissolution method to fabricate MgC_2O_4 of facile operation and rapid reaction, evaluated as a novel cathode in MLIBs. The XRD results of MgC_2O_4 revealed the crystalline nature of the material, and employing Scherrer's equation, it was possible to find the average size of the crystallites ≈ 26.88 nm. Furthermore, the SEM analysis indicated a cylindrical rod morphology. The results obtained by DTA were complementary to those obtained by FTIR. Meanwhile, the material in cycling performance at 10 mA g^{-1} delivered a high initial discharge capacity of 284 mAh g^{-1} with a coulombic efficiency above 99% for all cycles. Thus, the MgC_2O_4 has great potential as a candidate cathode material in Mg^{2+}/Li^{+} hybrid ion batteries for electricity storage. In addition, the use of these storage systems promotes sustainable development and contributes to environmental care by converting CO_2 to $C_2O_4^{-2}$.

Acknowledgments

The authors express their gratitude to Facultad de Ciencias Químicas, Universidad Autónoma de Nuevo León for their financial support and for providing access to laboratory equipment used in this project (Materials Laboratory 2) at División de Estudios de Posgrado. Jesús Guzmán-Torres would like to acknowledge Consejo Nacional de Ciencia y Tecnología for the scholarship awarded to support his PhD studies.

Declarations

Conflict of interest

The authors have disclosed no conflict of interest.

Supplementary Information

The online version contains supplementary material available at https://doi.org/10.1557/s43579-023-00438-y.

References

1. Z. Zhengxin, J. Taoli, A. Mohsin, M. Yahan, J. Yang, C. Yi, C. Wei, Chem. Rev. **122**, 16610 (2022)
2. C. Yuming, X. Maowen, H. Yunhui, M. Arumugam, Chem **8**, 312 (2022)
3. W. Zhenkang, C. Yufeng, Z. Jinqiu, L. Jie, S. Xiaowei, J. Haoqing, Y. Chenglin, Q. Tao, Energy Storage Mater. **47**, 122 (2022)
4. W. Chuanliang, T. Liwen, Z. Yuchan, W. Zhengran, F. Jinkui, Q. Yitai, Energy Storage Mater. **52**, 299 (2022)
5. W. Peiyu, Y. Xingbin, Energy Storage Mater. **45**, 142 (2022)
6. J.S. Yeoh, C.F. Armer, A. Lowe, Mater. Today Energy **9**, 198 (2018)
7. L. Nan, L. Qing, G. Xiaotian, Y. Meijuan, P. Huan, J. Chem. Eng. **372**, 551 (2019)
8. G.T. Jesús, L.O.G. Dalmy, L.G.T. Lorena, C.G.T. Luis, M.P.A. Salomé, G.J. Edgar, G. Idalia, M.S. Eduardo, J. Electron. Mater. **52**, 1250 (2023)
9. S.L. Reddy, T.R. Reddy, G.S. Reddy, T. Endo, R.L. Frost, Spectrochim. Acta A Mol. Biomol. Spectrosc. **123**, 25 (2014)
10. H. Kai, C. Nuofu, W. Congjie, W. Lishuai, C. Jikun, Cryst. Res. Technol. **53**, 1700157 (2018)
11. M.A. Friese, S. Banerjee, P.J. Mangin, Surface analysis of paper, 119 (2020)
12. V. Aikaterini, V. Anastasia, T. Ioannis, M.K. Pagona, G. Evangelos, J. Hazard Mater. **336**, 93 (2017)
13. K. Nakamoto, Wiley-Interscience Publication, (1997)
14. I.W. Sutapa, A.W. Wahab, P. Taba, N.L. Nafie, J. Orient. Chem. **34**, 1016 (2018)
15. I.W. Sutapa, A.W. Wahab, P. Taba, N. La Nafie, Indones. J. Fundam. Appl. Chem. **4**, 82 (2019)
16. K. Ashok, K. Jitendra, J. Phys. Chem. Solids **69**, 2764 (2008)
17. R.G. Rupard, P.K. Gallagher, Thermochim. Acta **272**, 11 (1996)
18. J. Yu, C. Hukui, M. Xiaxia, H. Zhijun, J. Phys.: Conf. Ser. **1653**, 012057 (2020)
19. Y.N. Zhang, S.S. Li, H.X. Kuai, Y.F. Long, X.Y. Lv, J. Su, Y.X. Wen, RSC Adv. **11**, 23259 (2021)
20. Z. Huang, Z. Jin, J. Lu, Y. Wang, S. Shi, W. Yin, J. Alloys Compd. **940**, 168808 (2021)
21. Q. Zhiqiang, W. Yuandong, L. Xiaofang, Q. Yi, Y. Yongying, M. Dajiang, Ionics **26**, 33 (2020)
22. M. Sebastian, J. Oleg, H.A. Abraham, G.G.M. Ignacio, B. Ronny, F. Johanna, S. Anatoliy, M. Alexander, E. Martin, M. Daria, A.C.S. Appl, Mater. Interfaces **13**, 6309 (2021)
23. A. Meidiana, P.H. Anjas, A. Enni, N.I. Muhammad, S.Y. Cornelius, Energy Storage Technol. Appl. **1**, 12 (2021)
24. S. Shaojun, H. Xiaoyan, G. Hongtao, Ceram. Int. **44**, 13495 (2018)
25. S. Fancheng, C. Tingting, L. Qing, P. Huan, J. Colloid Interface Sci. **627**, 483 (2022)
26. Z. Chi, Z. Binfeng, S. Zhi, S. Shaojun, M. Han, Ceram. Int. **46**, 1018 (2020)
27. L.Y. Xue, F.F. Xing, Y. Zhou, J. Su, Y.F. Long, Y.X. Lv, Y.X. Wen, J. Mater. Sci.: Mater. Electron. **33**, 8193 (2022)
28. Z. Zhiming, L. Peirong, Z. Shiqiang, J. Huile, Q. Yudan, A.C. Xi, T. Xinyue, Z. Qingcheng, G. Daying, W. Shun, Small **18**, 2205887 (2022)
29. Y. Li, G. Gao, Q. Wang, K. Zhang, Y. Yao, I.O.P. Conf, Ser.: Earth Environ. Sci. **692**, 022073 (2021)
30. G.J. Edgar, G.T. Jesús, G.G.D. Fabiola, G.G.D. Ixcoátl, P.A. Nayeli, G.T.L. Leticia, S.C.E. Maximino, J. Mater. Sci. **58**, 4082 (2023)